IEEE Access
Multidisciplinary | Rapid Review | Open Access Journal

Received August 6, 2020, accepted August 24, 2020, date of publication September 3, 2020, date of current version September 21, 2020.

Digital Object Identifier 10.1109/ACCESS.2020.3021673

Hot-Spot Temperature Forecasting of the Instrument Transformer Using an Artificial Neural Network

EDGAR ALFREDO JUAREZ-BALDERAS[1,2], JOSELITO MEDINA-MARIN[3], JUAN C. OLIVARES-GALVAN[4], (Senior Member, IEEE), NORBERTO HERNANDEZ-ROMERO[3], JUAN CARLOS SECK-TUOH-MORA[3], AND ALEJANDRO RODRIGUEZ-AGUILAR[1,2]

[1]Postgrado de CIATEQ, A.C., Cd. Sahagún, Hidalgo, C.P. 43990, México
[2]Arteche North America S.A. de C.V., Tepeji del Río de Ocampo, Hidalgo, C.P. 42855, México
[3]Centro de Investigación Avanzada en Ingeniería Industrial, Universidad Autónoma del Estado de Hidalgo, Pachuca, Hidalgo, C.P. 42184, México
[4]Departamento de Energía, Universidad Autónoma Metropolitana, Azcapotzalco, Ciudad de México, C.P. 02200, México

Corresponding author: Joselito Medina-Marin (jmedina@uaeh.edu.mx)

This work was supported in part by the Consejo Nacional de Ciencia y Tecnología (CONACYT) in coordination with the Postgrado de CIATEQ, A. C., Mexico; in part by the Universidad Autónoma del Estado de Hidalgo under Project CONACYT CB-2017-2018-A1-S-43008; in part by the Universidad Autónoma Metropolitana; and in part by the company Arteche North America, S. A. de C. V.

ABSTRACT Cast resin medium voltage instrument transformer are highly used because of several benefits over other type of transformers. Nevertheless, the high operating temperatures affects their performance and durability. It is important to forecast the hot spots in the transformer. The aim of this study is to develop a model based on Artificial Neural Networks (ANN) theory to be able to forecast the temperature in seven points, taking into account twenty-six input data of transformer design features. 792 simulations were carried out in COMSOL Multiphysics® to emulate the heat transfer in the transformer. The data obtained were used to train 1110 ANN with different number of neurons and hidden layers. The ANN with the best performance ($R = 1$, MSE $= 0.003455$) has three hidden layers with 10, 9 and 9 neurons respectively. The ANN predictions were validated with finite element simulations and laboratory thermal tests which present similar patterns. With this accuracy in the prediction of hot-spot temperature, this ANN can be used to optimize the design of instrument transformers.

INDEX TERMS Artificial neural networks, resin-cast instrument transformer, epoxy resins, finite element analysis, hot-spot temperature.

I. INTRODUCTION

Instrument transformers are important assets, used throughout the transmission and distribution networks for monitoring voltages and currents [1]. Dry-type instrument transformers made of cast resin are highly suitable over oil isolated transformers in many operations due to several advantages such as mechanical and dielectric properties, heat resistance, non-flammability, etc. [2], [3]. They are also extensively used in commercial and industrial settings [4]. However, the low thermal conductivity in dry-type instrument transformers results in high operating temperatures, directly influencing their performance and service life [2], [5].

The associate editor coordinating the review of this manuscript and approving it for publication was Ramakrishnan Srinivasan.

Figure 1 illustrates the construction of a cast resin dry-type medium voltage instrument transformer manufactured for indoor service. The windings are manufactured with double enamel copper wires; the core is built of silicon steel and the lamination is of grain-oriented type with high permeability and low losses; the core and windings are encapsulated in epoxy resin that provides excellent dielectric properties and mechanical resistance [6].

Manufacturers usually design dry-type instrument transformers to operate at ambient temperature with permanent loading capacity [4]. However, external temperature instability, electrical characteristics, resin property and degradation of the transformer internal insulation can lead to undesirable thermal performance [3].

Over the years, several research works have been previously carried out to study the temperature distribution

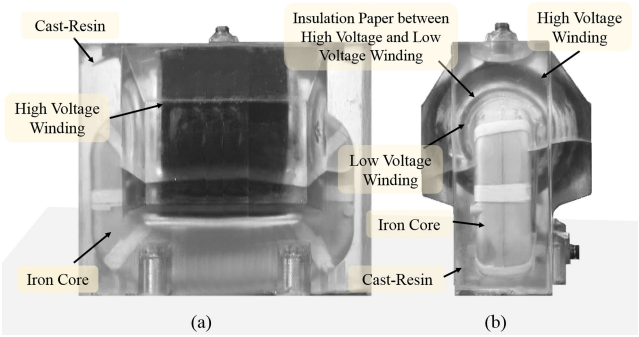

FIGURE 1. Radiographic image of a Dry-type medium voltage instrument transformer for indoor service. (a) Transformer transverse view. (b) Transformer front view.

and hot spots in transformers. Heat transfer phenomena in the transformer involve thermal conduction, convection, and radiation; hence, a very complicated theoretical equation set is necessary to predict the temperature in transformers [3]. There are several research works reported in the literature regarding temperature in transformers, such as equivalent circuit [7]–[9], finite element analysis-based modeling and simulations [10]–[12], and experimental works [13]–[15]. However, the operational properties of each transformer are subject to its geometry, materials, electrical characteristics, etc.

In [16], the authors proposed a method to forecast the temperature of hot spots in oil-immersed transformer windings; it includes an ANN with only one hidden layer and a value of R very close to one; this ANN is used to predict the transformer temperature in different hot spots. In our work, we are considering a dry-type instrument transformer to forecast its hot spots, not only in windings but also in core and internal insulation of transformer taking into account environmental conditions for ANN training, and we have done lab studies with a transformer prototype manufactured for this purpose. Moreover, to be able to find the ANN with the best performance, our search algorithm creates ANNs with one to three hidden layers, and a sensitivity analysis was carried out to identify the influence of input variables in the model.

Artificial Neural Networks (ANNs) have been applied for modeling and analyzing different type of systems. The usage of an ANN for modeling transformers has advantages over some other techniques. For example, ANNs can handle several input and output variables of the system that is being modeled. In addition, highly complex classification problems can be solved with the study of heat transfer in a very efficient manner and in less processing time to provide a feasible solution to the problem. It is achieved because ANNs can separate non-linear decision regions as complicated as desired depending on the number of neurons and layers with a simple structure. Taking into account these advantages, it was decided to use ANN theory in this study because it allows the construction, modification and representation of complex models without the need of advanced mathematical modeling, and the results can be ideal for the study and/or design of transformers.

No paper has been published that uses an ANN to forecast temperatures and hot spot in a dry-type instrument transformer considering all possible combinations of geometric, electrical and mechanical design variables, as a result, this article describes a procedure for configuring a thermal model in cast resin dry-type medium voltage instrument transformers using ANNs. Therefore, the main contribution of this research is the methodology for obtaining ANNs with a high performance for predicting the maximum temperature in the low and high voltage winding, core, transformer body (epoxy resin), insulation between high and low voltage (paper), as well as the boundary between the transformer body and the environment. The ANN model can be used to study the temperature distribution, and hot spots, providing a tool that can help in designing medium voltage instrument transformers.

The results of this methodology based on ANN are validated by comparing them with finite element simulations and laboratory tests carried out on a prototype built especially for this research. The ANN model is accurate and efficient enough for practical application at the design stage. Figure 2 shows a flowchart of the methodology used for this research work, from the design of the transformer until the ANN validation.

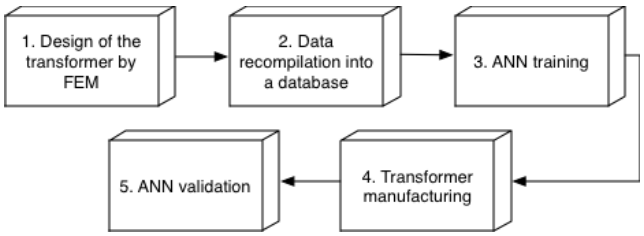

FIGURE 2. Flowchart of the methodology applied in this research work.

The rest of this article is structured in the following order. Firstly, the structure of a cast resin dry-type medium voltage instrument transformer is described in section II. Section III presents the thermal models governing the temperature behavior in transformers. In section IV, the heat sources of this type of transformers are identified. Section V describes the modeling process for transformers through finite element method (FEM). The process to obtain the ANN with the best performance is presented in section VI. Then, section VII shows the validation of the ANN in a physical model. Finally, section VIII concludes the paper.

II. THE TRANSFORMER GEOMETRY

The geometry of cast resin dry-type medium voltage instrument transformer patented in [6], was manufactured for this research work. The geometrical arrangement of the transformer under study is shown in Figure 3. The magnetic core is made up of magnetic laminations of silicon steel forming

a cross-section block, the primary and secondary windings are insulated with dielectric cardboard sheets. The secondary winding is placed over a magnetic core, while the primary winding is placed over the secondary winding. The insulation between high and low voltage windings is diamond-dotter paper and the core and the windings are encapsulated with epoxy resin [6].

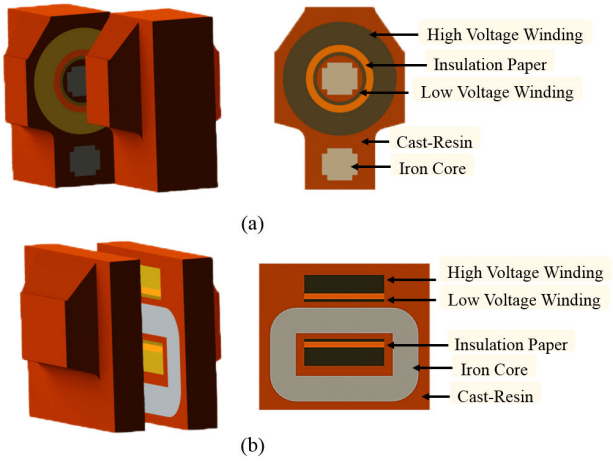

FIGURE 3. Geometric detail of the Dry-type medium voltage instrument transformer for indoor service. (a) Front Cut. (b) transversal cut.

By taking into account the geometric dimensions obtained from the transformer design calculation algorithm, maximum temperatures can be more accurately predicted. In this research work, the three-dimensional (3D) geometry of the transformer is considered. Additionally, a simple and easy-to-operate parametric design is carried out to adapt the geometrical characteristic of the components of the transformer under study. Figure 4 shows the block diagram of the parametric design system developed. The parameterization process includes the extraction of geometric variables and parameters from the transformer calculation algorithm.

Parametric design is the basis for creating mathematical and geometric relationships that allows the deriving of automated process variables and parameters. The parameters and initial variables (electrical, magnetic, mechanical, geometric and environmental) will guide the generation of output variables (temperatures and hot spots in the transformer).

III. HEAT TRANSFER

The thermal models used to study the temperature distribution and to know the hot spots in the transformer have been analyzed and developed in multiple engineering disciplines, such as electrical circuit theory, fluid dynamics, numerical methods, electromagnetic theory, etc. Each thermal model has its own applications. However, these thermal models have one thing in common, which is the study of heat propagation. Radiation, convection, and conduction are considered the fundamental pillars in the study of heat transfer in the transformer [3], [17]; hence, a complex theoretical set of equations is required to predict temperature [3].

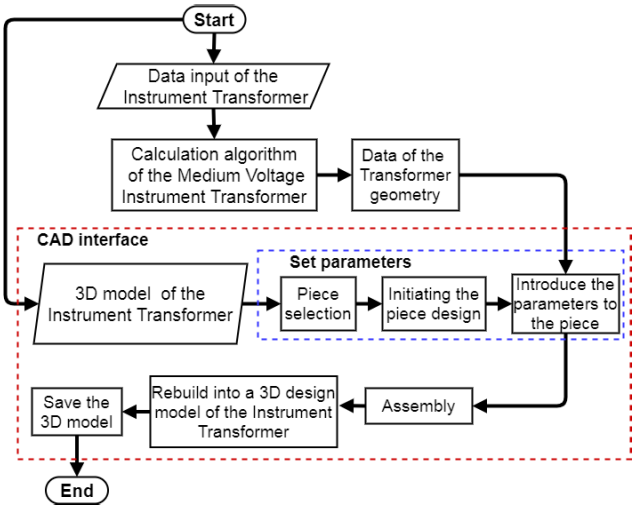

FIGURE 4. Block diagram of the parametric design system.

The temperature distribution inside the cast resin dry-type medium voltage instrument transformer manufactured for indoor service (Figure 1) can be obtained by solving (1) - (3), which are derived from the energy conservation law [18], [19].

In this study, we consider radiation, convection, conduction in steady state analysis to predict the temperature in the instrument transformer. The initial temperature in the transformer body is considered to be the same as the environmental temperature, and the heat convection and radiation, shown in (2) and (3), are used as boundary conditions [11], [18], [19].

$$c\rho\frac{\partial T}{\partial t} = \frac{\partial}{\partial x}\left(k\frac{\partial T}{\partial x}\right) + \frac{\partial}{\partial y}\left(k\frac{\partial T}{\partial y}\right) + \frac{\partial}{\partial z}\left(k\frac{\partial T}{\partial z}\right) \quad (1)$$

$$\frac{dQ_{conv}}{dt} = h(T_s - T_\infty) \quad (2)$$

$$\frac{dQ_{rad}}{dt} = \varepsilon\sigma T_S^4 - \alpha G \quad (3)$$

In the stationary state, the term $\partial T/\partial t$ in equation (1) is equal to zero; therefore, equation (1) can be expressed as below [20]:

$$\nabla^2 T_{(x,y,z)} = \frac{Q}{k} \quad (4)$$

where: k is the thermal conductivity (W/(m°C)), Q is the heat source (W/m^3), ρ is the mass density (kg/m^3), C is the specific heat (J/(kg°C), T is the temperature (°C), t is the time (s), Q_{conv} and Q_{rad} are the rates of heat transfer per unit area on the surface by convection and radiation (W/m^2), respectively, h is the convective heat transfer coefficient (W/(m^2°C), ε is the emissivity of the surface, σ is Stefan-Boltzmann's constant (W/(m^2 °C^4)), α is the absorptivity, G is the irradiation (W/m^2), T_s is the surface temperature (°C) and T_∞ is the environment temperature.

At the same time, natural convection occurs due to the buoyancy forces caused by differences in fluid density due to temperature variation. That is why the convective heat

transfer coefficient h depends on the geometry of the transformer surface. In addition, thermal radiation is calculated by differentiating the energy emitted on the surface of the transformer (solid) from the energy incident on the surface (ambient temperature). Emissivity and absorptivity in equation (3) are the surface properties determined according to the geometry and material of the surface. However, the heat sources described in equation (1), and equation (2) represent uniform heating due to core losses and winding losses; the heat generation per unit volume can also be obtained by equation (5) [21], [22].

$$Q = \frac{P}{V} \tag{5}$$

where: Q is the heat source (W/m^3), P is the loss in the core and in the windings (W), and V is the volume of the heat source (m^3).

IV. HEAT SOURCES IN THE TRANSFORMER

In dry-type medium voltage instrument transformers such as the one illustrated in Figure 1, the primary and secondary windings are made of copper; hence, they offer high thermal conductivity [10].

In addition, once the transformer is energized and exposed to environmental temperature, the energy losses in these components (core and windings), and together with convection and solar radiation from the atmosphere in the transformer body, heat-generating sources are established inside and outside the transformer [23]–[25].

Figure 5 illustrates the heat sources inside the cast resin dry-type medium voltage instrument transformer manufactured for indoor service.

The energy losses in high voltage winding (equation (6)) and low voltage winding (equation (7)) can be obtained independently considering the winding geometry, length, cross-section resistance and resistivity of the conductive material [26]. In addition, for a transformer, the sum of copper losses can be obtained by equation (8) [27], [28].

$$P_{cu_1} = R_1 I_1^2 = \rho_1 \left(\frac{l_1}{s_1}\right) I_1^2 \tag{6}$$

$$P_{cu_2} = R_2 I_2^2 = \rho_2 \left(\frac{l_2}{s_2}\right) I_2^2 \tag{7}$$

$$P_{cu} = \sum_{i=1}^{n=2} P_{cu_i} \tag{8}$$

where: P_{cu_1} are the primary winding losses (W), P_{cu_2} are the secondary winding losses (W), P_{cu} represent the total winding losses due to the Joule effect (W), R_1 is the resistance of the conductor material in the primary winding (Ω), R_2 is the resistance of the conductor material in the secondary winding (Ω), ρ_1 is the resistivity of the conductor in the primary winding (Ω.m), ρ_2 is the resistivity of the conductor in the secondary winding (Ω.m), l_1 is the length of the conductor in the primary winding (m), l_2 is the length of the conductor in the secondary winding (m), S_1 is the conductor cross sectional area in the primary winding (m^2), S_2 is the conductor cross sectional area in the secondary winding (m^2), I_1 is the current in the primary winding (A), and I_2 is the current in the secondary winding (A). The core losses depend on the material type (Silicon Steel, Amorphous, Crystalline Nano, etc.), the frequency, material thickness and the flux density at which it operates; these losses are given by equation (9) [29], [30].

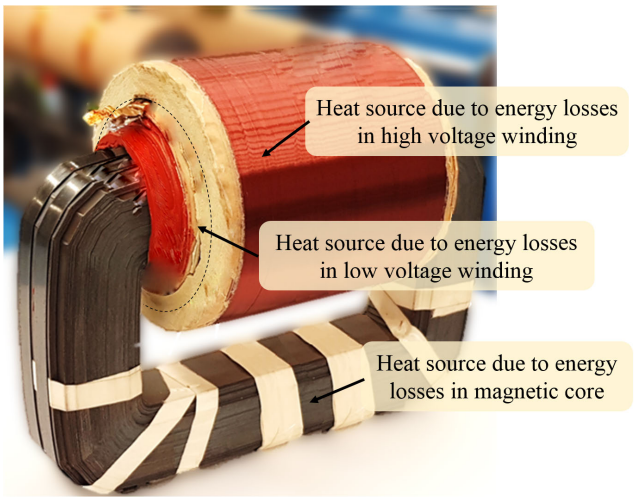

FIGURE 5. Sources of heat generated inside the instrument transformer of medium voltage dry-type cast resin manufactured for indoor service.

$$P_c = k_c B^{\alpha} f^B \tag{9}$$

where: P_c is the specific core losses (Watts/kg), B is the magnetic flux density (T), f is the frequency (Hz), the constant k_c, α, B, can be established from the datasheets of the material manufacturer [30]. Moreover, the core losses are classically composed of hysteresis losses and eddy current losses, which can be expressed by equation (10).

$$P_C = P_h + P_e = \delta_h f B^2 + \delta_e f^2 B^2 \tag{10}$$

where: P_h are the hysteresis losses in the core (W), P_e are the eddy current losses in the core (W), δ_h and δ_e are constants which are material depend, and f is the frequency (Hz).

For this study, we use the loss curve at 60 Hz (reported in [5], [31]) in the calculation algorithm of the transformer design to determine the losses in the core.

Transformer losses can be expressed by equation (11) [3].

$$P = P_{cu} + P_C \tag{11}$$

where: P are the total losses of the transformer (W), P_{cu} is the total winding losses due to the Joule effect (W) and P_C is the core losses (W).

V. MODELING THROUGH FINITE ELEMENT METHOD

During a stable electrical load in the medium voltage instrument transformer (Figure 1), the internal losses (equation 11) and the heat generated by the environment (equations

2 and 3) increase or decrease the transformer temperature. For thermal analysis, a 3D model of the transformer geometry is implemented and the temperature distribution and hot spots are simulated.

The FEM is used to solve the equations of stable state energy, i.e. equations (1) to (4) are solved, for obtaining the thermal behavior of heat transfer and the hot spots in the internal parts of the transformer and in the transformer housing.

The FEM has some advantages in the modeling of complex systems, such as modeling of complex geometries, boundary conditions can be easily incorporated, different types of materials can be incorporated into the modeling, each domain of geometry can be applied elements of different order, among others. However, it has some drawbacks, such as a large amount of data is required as input to generate the mesh, it depends on a nodal connectivity and parameters depending on the type of problem, it requires a computer of great capacity to give solution to the equations of each node, among others. Notwithstanding the drawbacks, FEM has features that helps in the modeling of dry-type instrument transformers.

For the analysis, the heat transfer module of COMSOL Multiphysics® software was used. The software is based on solving the heat transfer problem according to the parameters and variables defined in the instrument transformer calculation algorithm. Moreover, the software internally performed the matrix representation for each transformer element, the formation of the global coefficient matrix, and the application of the initial and boundary conditions to solve the thermal problem [21].

By using a computer program implemented in COMSOL Multiphysics®, several simulations were carried out modifying the electrical and geometric characteristics of the transformer.

Considering that transformers, like all electrical and electronic equipment, is constantly being modernized and that in the industry transformers of different shapes, sizes, materials, core configurations, dielectric distances, etc. are designed, manufactured and marketed, and are subjected to different environmental conditions, it was decided to take for this investigation the primary input variables that are part of the design requirement for an instrument transformer.

Table 1 shows the properties of the materials associated with the 3D computational model of the transformer geometry [32], while Table 2 and Table 3 show the input and output variables that are introduced into the proposed computational program to provide a solution to the heat transfer model in the instrument transformer.

According to statistics presented in [33] about the failure location distribution, the major failure sources in transformers come from the winding and core (>40%). In this article, we are focused in seven variables related to temperature, the maximum temperature in the internal parts of the transformer (Y_1 to Y_4), the maximum and minimum resin temperature (Y_5 and Y_6, respectively), and the maximum temperature in the contour of the transformer (Y_7) that is in contact with the atmosphere. These temperatures are correlated to transformer features and environment temperature, grouped in twenty-six variables described in Table 2. In addition, the determination of Y_7 is of great importance because they can be estimated for the measurement of the ohmic resistance in the thermal test of the transformer and, at the same time, the maximum temperature rise in the primary and secondary winding can be forecasted by using the method of resistance variation.

In this article, 792 simulations were performed combining the input parameters, whose ranges are shown in the third column of Table 2. The materials are considered isotropic in all simulations. In addition, copper was used in the windings and silicon steel for the core, and the loss curve (60 Hz) reported in [5] was also considered.

Figure 6 shows the tetrahedral mesh in all domains of the transformer including the environment (2'693,508 tetrahedral elements in all domains). Figure 7 shows some of the results of the simulations obtained and the computer program designed to automatically modify the electrical and geometric characteristics of the transformer. It also visualizes the thermal behaviors in a stable state with different environmental temperatures.

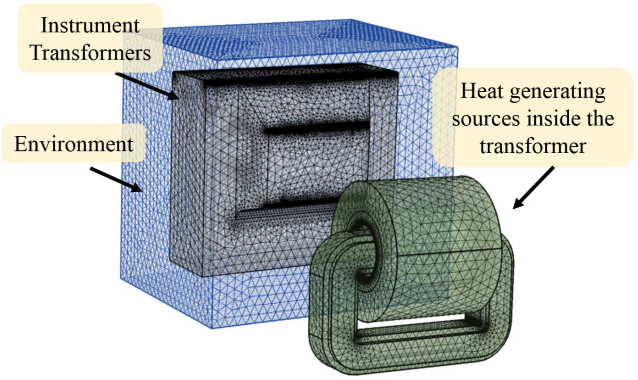

FIGURE 6. Mesh density using tetrahedral elements in all domains of the transformer including the environment to provide a solution to finite element analysis and consequently to thermal behavior.

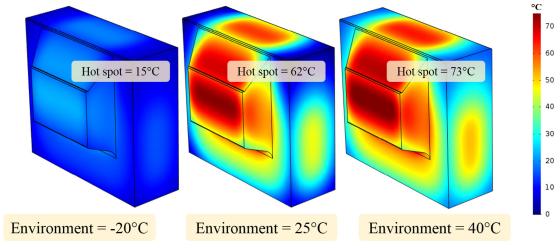

FIGURE 7. Distribution of the calculated temperature in the body of the Medium Voltage Instrument Transformer and location of the hot spot at different environmental temperatures.

Figures 8 and 9 show the block diagram and flowchart of the computer program of the proposed methodology, respectively. In these diagrams, the integration of the algorithm

for calculating the design of the transformer, the parametric design system and the 3D computational model of the geometry of the transformer are shown. Moreover, the initial and boundary conditions related to the environment are set in the diagram. The data obtained after each iteration are stored in a database, which was used to train the ANN.

TABLE 1. Properties of the materials [32].

Material	K (W/(m^{o}K))	C (J/(kg^{o}K)	ρ (kg/m^3)
Copper	400	385	8700
Silicon steel	50	420	7000
Insulation systems	0.24	1564	1714

TABLE 2. Input variables that are considered in the transformer calculation algorithm and saved in the database.

Input Variable	Name of the variable	Study parameter
X_1	Primary voltage (V)	2400, 5040, 8400
X_2	Secondary voltage (V)	120
X_3	Number of primary turns	2440 to 16170
X_4	Number of secondary turns	122, 154, 231
X_5	Primary winding inner diameter (mm)	95
X_6	Primary winding outer diameter (mm)	$\leq$ 165.58
X_7	Secondary winding inner diameter (mm)	65
X_8	Secondary winding outer diameter (mm)	$\leq$ 93.11
X_9	Primary winding height (mm)	15.12 to 70.58
X_{10}	Secondary winding height (mm)	0.82 to 28.11
X_{11}	Primary winding layers	12 to 57
X_{12}	Turns per layer in the primary winding	107 to 743
X_{13}	Primary wire (AWG)	18 to 36
X_{14}	Secondary wire (AWG)	8 to 36
X_{15}	Frequency (Hz)	50 and 60
X_{16}	Magnetic induction (Teslas)	1.0 to 1.9
X_{17}	Number of primary winding papers	6 to 21
X_{18}	Primary wire cross-section (mm^2)	0.823 to 0.0113
X_{19}	Secondary wire cross-section (mm^2)	8.367 to 0.0113
X_{20}	Primary resistance (Ω)	20.33 to 8587.44
X_{21}	Secondary resistance (Ω)	0.062 to 76.785
X_{22}	Applied test voltage (kV)	38
X_{23}	Losses in primary winding (W)	4.14 to 117.93
X_{24}	Losses in secondary winding (W)	0.037 to 41.96
X_{25}	Core losses (W)	4.186 to 22.54
X_{26}	Environment temperature (^{o}C)	-20, 20, 60

TABLE 3. Output variables that are considered in the transformer calculation algorithm and saved in the database.

Output Variable	Name of the variable
Y_1	Maximum temperature in primary winding (^{o}C)
Y_2	Maximum temperature in secondary winding (^{o}C)
Y_3	Maximum temperature in the insulation between primary and secondary winding (^{o}C).
Y_4	Maximum core temperature (^{o}C)
Y_5	Maximum temperature in the epoxy resin (^{o}C)
Y_6	Minimum temperature in the epoxy resin (^{o}C)
Y_7	Maximum contour temperature resin - environment (^{o}C)

VI. ARTIFICIAL NEURAL NETWORK DESIGN

Smart computing tools are powerful in monitoring, diagnosing and evaluating the life of transformers [34]. ANNs are a branch of computer intelligence, consisting of a set of computational units known as neurons that are highly interconnected in a specific topology. In addition, ANNs are able to learn and have been successfully used in a wide spectrum of applications [35].

Despite an ANN has some drawbacks, such as an unexplained behavior of the network, the identification of the correct structure, the hardware dependence, among others, it has many advantages. ANNs can create models with incomplete knowledge, are fault tolerant, have distributed memory and parallel processing capability, among others.

In this section, the design of an ANN is presented. The obtained ANN has the ability to predict the maximum temperature in the components of the resin cast dry-type medium voltage instrument transformer, manufactured for indoor service.

The ANN design was developed using the Neural Network Toolbox in MATLAB®. A script was implemented for searching the optimal configuration of neurons and hidden layers to minimize the Mean Square Error (MSE) and obtain a correlation curve (R) between input and output data.

The number of neurons (NN) per layer and the number of hidden layers (HL) give the guideline to perform several possible combinations in search of an optimized topology, where the MSE should be near zero and R between the input and output data should be close to one. It is important to note that in a multi-layer perceptron topology all the layers are connected to each other, as shown in Figure 10.

The input data used for the ANN design corresponds to the variables and parameters of the transformer design represented in Table 1. This data and the results of the COMSOL Multiphysics® simulations were saved in a database and used to train and validate the ANNs generated in Matlab®.

In order to have a wide spectrum of possibilities, in this research work we have analyzed ANNs which contain one, two or three hidden layers. Equation (12) was used to estimate the number of all possible combinations for the ANN configuration. Considering from one to ten the NN per each HL, with one HL we have 10 possibilities, with two HLs we get 100 ANNs, and so on. In this research work, a total of 1110 ANNs were trained using three HLs as maximum.

The learning algorithm considered in the ANN design is derived from the Least-Mean-Square (LMS), principle where the MSE is determined as the result of the difference between the target output and the network output (Equation 13) [16], [36].

$$j = \sum_{k=1}^{HL} (NN)^k \tag{12}$$

$$MSE = \frac{1}{m} \sum_{i=1}^{m} (t_i - y_i)^2 \tag{13}$$

The learning algorithm LMS has set of samples of the desired behavior: $\{x_1, t_1\}, \{x_2, t_2\}, \ldots \{x_m, t_m\}$ where the aim is to reduce the average sum of these errors; moreover, the LMS algorithm environment sets the weight and bias of the network to reduce the MSE [16], [36]; in this case, x_m

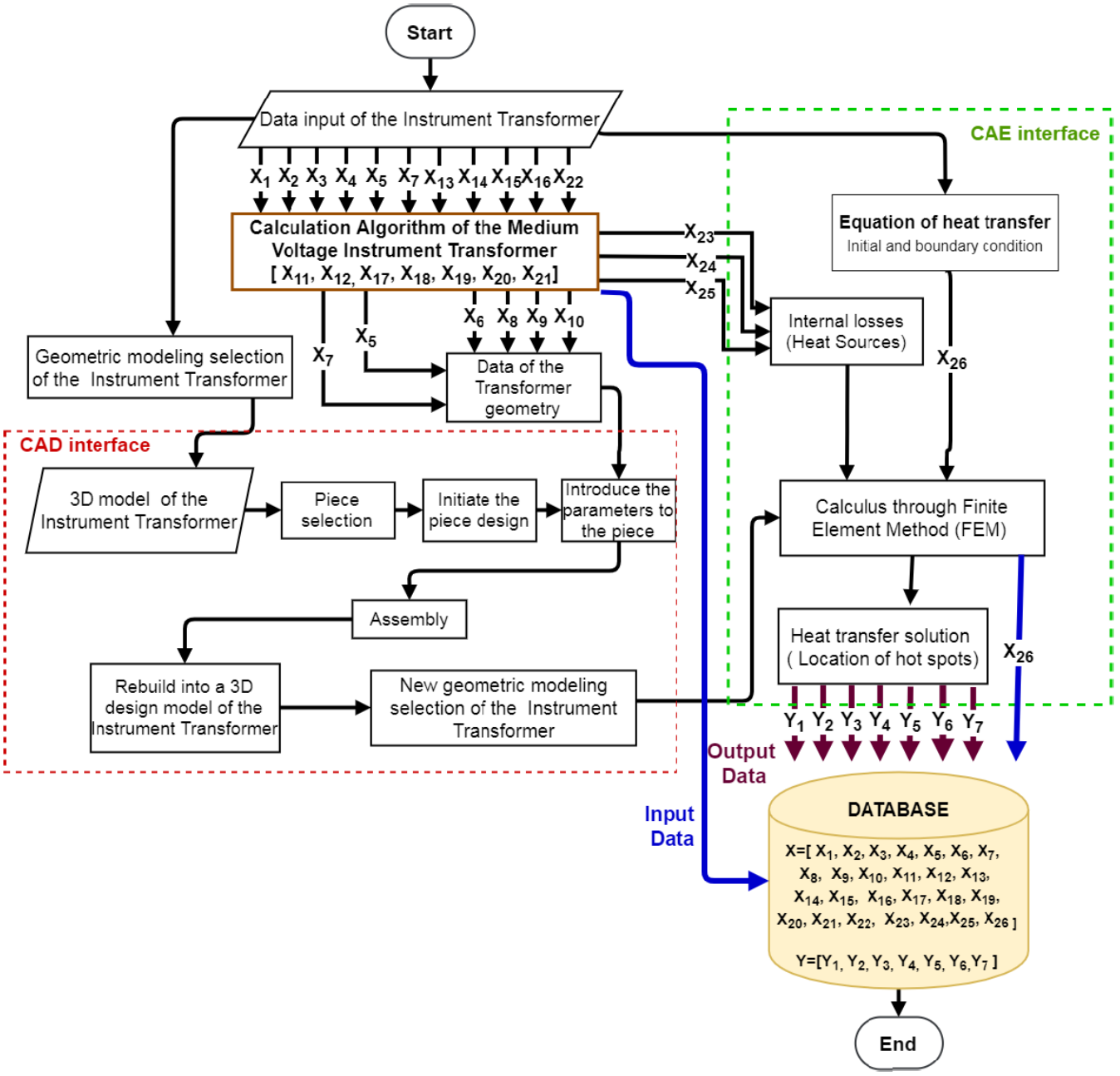

FIGURE 8. The block diagram proposed to generate the simulation results and stored in a database.

values are the network inputs, and t_m values are the respective targets. For every input in the net, the output is compared with the target [36].

The training process of the ANN starts with random weights, which are adjusted iteratively to reduce the MSE. The set of weights that minimize the error function is considered a solution to the system that represents the ANN [36]. Figure 11 shows the flowchart of the algorithm developed in MATLAB to implement the thermal behavior of the instrument transformer; and Figure 12 shows the obtained ANN, considering the twenty-six input variables and the seven output variables shown in Table 1 and Table 2. The size of the database consists of 792 simulations based on the FEM, that is, 792 records obtained from the same number of simulations. The inputs and outputs of these simulations were used to build the database used for the ANNs training. There was not necessary to normalize these data for the ANN training process due to the obtained ANNs showed a good performance from the original range of values. The configuration for the ANN with the best performance is (10:9:9), i.e., ten neurons in the first hidden layer and nine neurons in the second and the third ones.

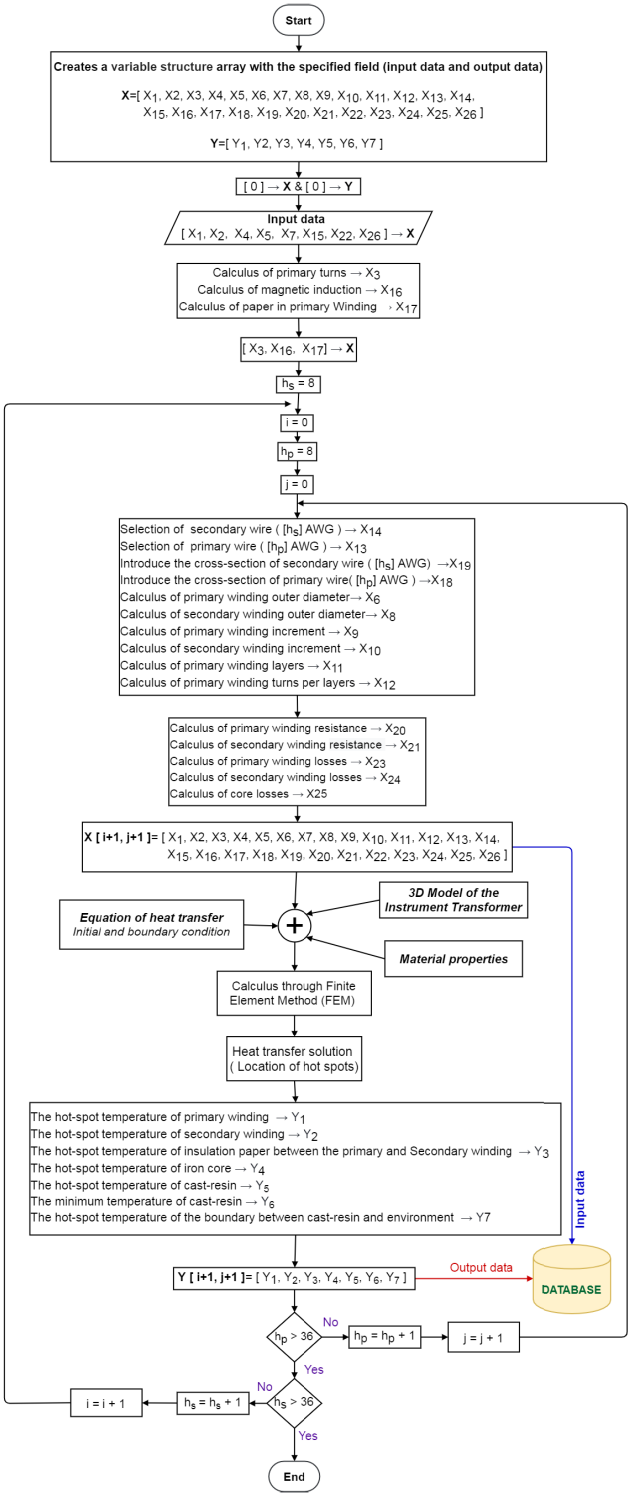

FIGURE 9. Flowchart of the proposed computational program to generate and save the simulation results.

The input data used to obtain the ANNs were divided into three groups: training data set (70%), verification data set (15%) and validation data set (15%). The sigmoid function is used in all layers to update weight and bias values according to Levenberg-Marquardt backpropagation algorithm. This

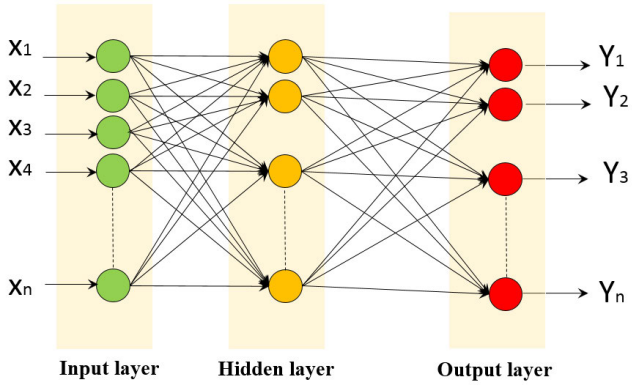

FIGURE 10. Multi-layer perceptron topology of ANN implemented for temperature study of cast-resin transformer.

function has been utilized widely in several applications of ANNs because of its effectiveness and rapidness in the back-propagation algorithm. On the other hand, a linear function is used in the output layer.

The results of ANN training are shown in Figures 13 and 14. Figure 13 shows the performance of the ANN training process with a MSE of 0.003455 in 1000 epochs. Figure 14 shows the correlation between the ANN outputs and the data used as targets, $R = 1$ proves the linearity of the RNA model.

The values predicted by the best qualified ANN for output variables were compared against the values obtained from COMSOL Multiphysics®. Figures 15 to 21 show the correlation between these values. It can be observed, in a graphical way, that the ANN predicts the temperature values of the seven variables of interest very close to those obtained by simulation. This fact is a good evidence that ANNs can be used to forecast the temperature behavior in transformers with high certainty. Table 4 shows the MSE for each value obtained from the ANN. Due to the high range of possibilities in transformer design with respect to its inputs, the temperatures were plotted with regard to the volume of each transformer component (Figure 15 to Figure 20) and superficially with regard to the boundary between the transformer body and the environment (Figure 21)

TABLE 4. MSE between the values calculated in COMSOL Multiphysics® and the values obtained from the ANN for each output variable.

Output Variable	MSE
Y_1	0.0051
Y_2	0.0043
Y_3	0.0062
Y_4	0.0027
Y_5	0.0081
Y_6	0.0022
Y_7	0.0134

A. SENSITIVITY ANALYSIS OF THE INPUT-OUTPUT EFFECT

A sensitivity analysis was carried out in order to verify the impact of each input variable in the ANN model. First,

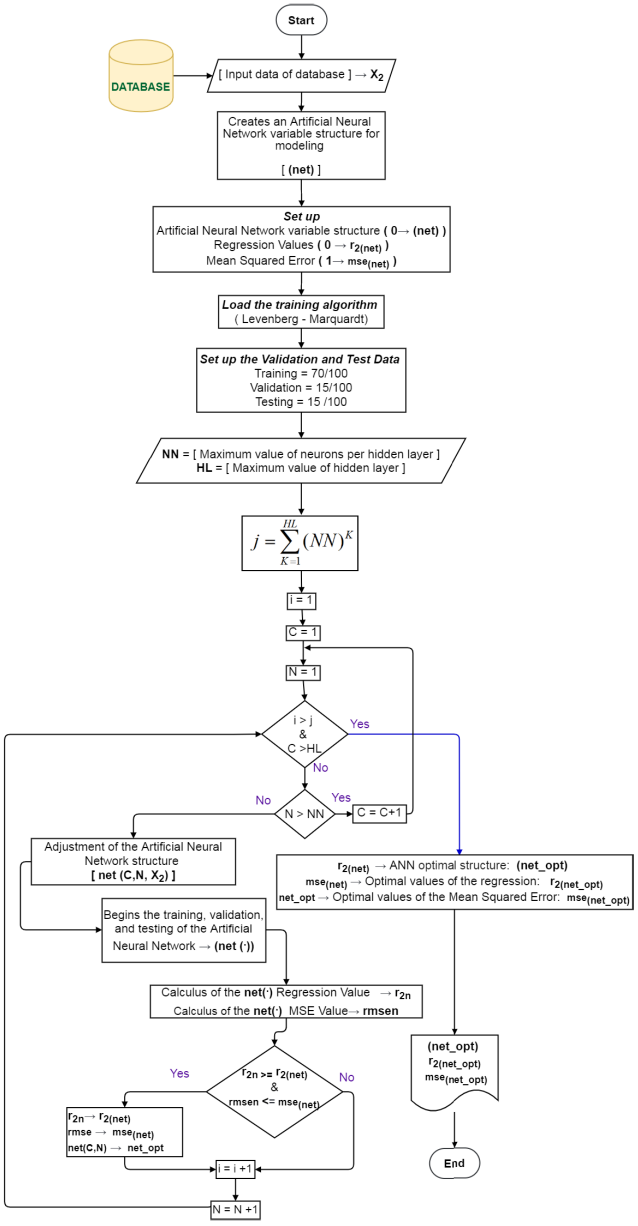

FIGURE 11. Flowchart developed for the search of ANN that models the thermal behavior of the instrument transformer.

we calculate the *MSE* with all the input variables. After that, we predict the output values omitting one input variable, then we obtain the corresponding MSE. This step is repeated for each input variable to determine its respective MSE_i. Equation 14 is used to calculate the sensitivity of the model for every input variable.

$$S_i = \frac{MSE_i}{MSE} \tag{14}$$

where: S_i: Sensitivity of the model to variable x_i; MSE_i: *MSE* of predicted values without data for input variable x_i; *MSE*: is the mean square error of predicted values taking into account all the input variables. Table 5 and Figure 22 show the sensitivity value for each input variable. The bigger value

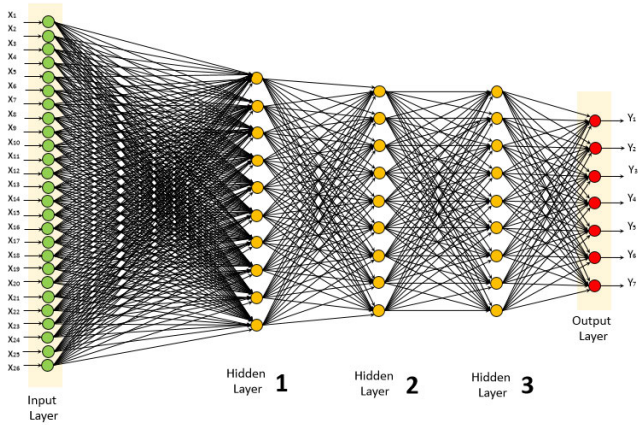

FIGURE 12. ANN structure that models the thermal behavior of the instrument transformer utilizing the input and output variables given in Tables 1 and 2.

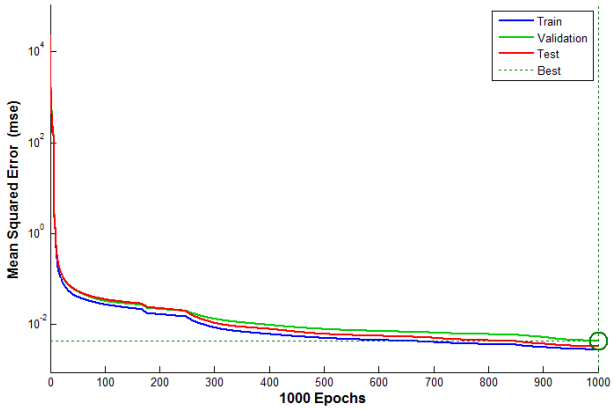

FIGURE 13. Performance of the ANN training process that models the thermal behavior of the instrument transformer.

S_i the more impact has variable x_i in the ANN model. In this case, variable X_{15} (frequency) presents the highest value and, in consequence, the highest impact in the model.

VII. EXPERIMENTAL VALIDATION

A physical model was manufactured in order to validate the output data predicted by the ANN with the best performance. A heating test was performed on a cast resin dry-type medium voltage instrument transformer manufactured for indoor service with similar characteristics shown in Figure 1, Figure 3 and Table 1. The standards IEC 61869-1 and IEC 61869-3 were followed during the heating tests. The instruments used in the test were: an ac voltage variator, a reactor, mercury thermometers, pyrometers and digital multimeters, as well as a digital hydro thermometer clock and type J thermocouples with fiberglass lining and stainless-steel mesh. Figure 23 shows the instrument transformer of cast resin medium voltage manufactured for indoor service at the time the heating test is applied. The transformer was similar to those provided for indoor service. Figure 24 shows the heating test diagram.

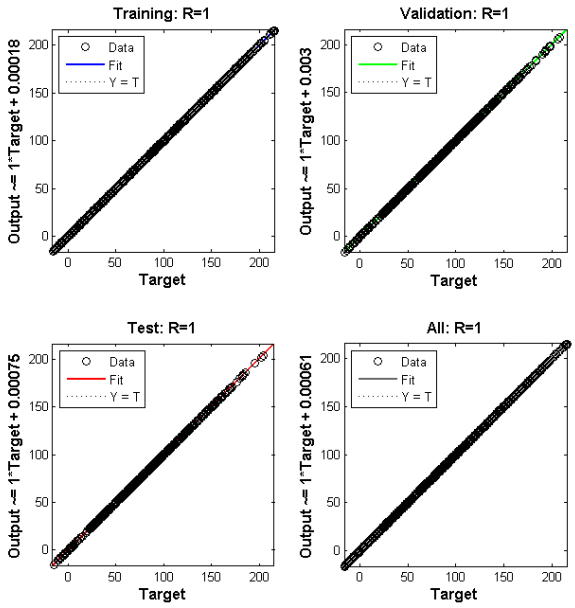

FIGURE 14. Correlation values (R) between input and output data of the ANN modeling the thermal behavior of the instrument transformer.

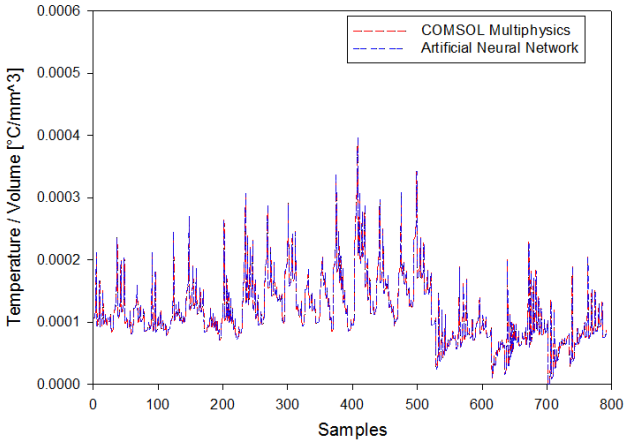

FIGURE 15. Maximum temperature variation according to the volume of the primary winding.

However, being a cast resin transformer and lacking sensors to measure the temperature inside the transformer, the temperature between the resin (transformer body) and the environment was taken into account for this research work.

The heating of the primary and secondary windings was calculated by the resistance variation method, according to standard IEC 61869-1 and IEC 61869-3 and the heating of the other parts was measured by thermocouples.

On the other hand, the transformer was tested at 1.0, 1.2, 1.5, 1.7, and 1.9 times the nominal voltage of high-voltage winding. In all the cases, stable thermal conditions were achieved, i.e., stabilization was obtained when the temperature difference of the thermocouples on the transformer resin wall and the average temperatures with respect to the

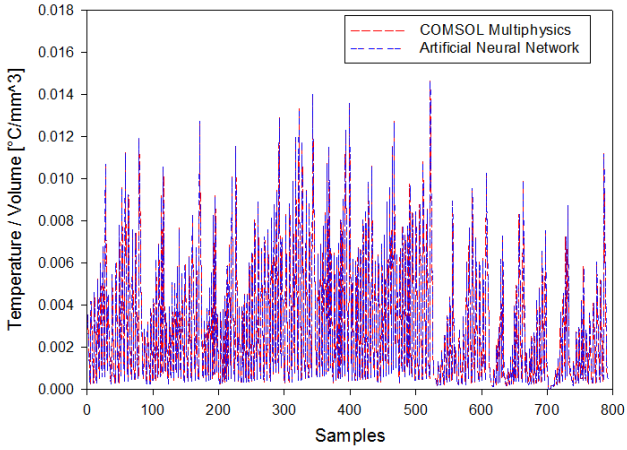

FIGURE 16. Maximum temperature variation according to the volume of the secondary winding.

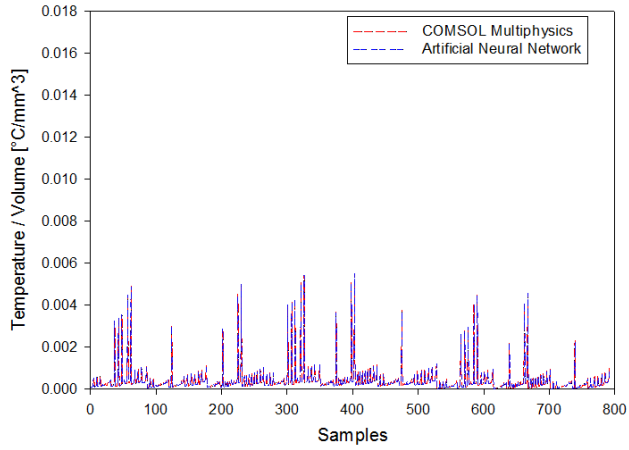

FIGURE 17. Maximum temperature variation according to the volume of the insulation between the primary and the secondary.

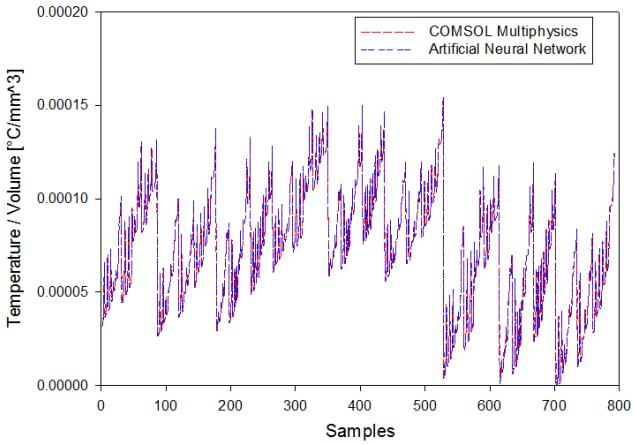

FIGURE 18. Maximum temperature variation according to the volume of the magnetic core.

environment did not vary by 1°C during three consecutive readings in a 30-minute interval.

The used values of the resistors load in the secondary winding was according to the heating power of the transformer. Once the temperature of the transformer was stabilized, the hot ohmic resistance of the high voltage winding

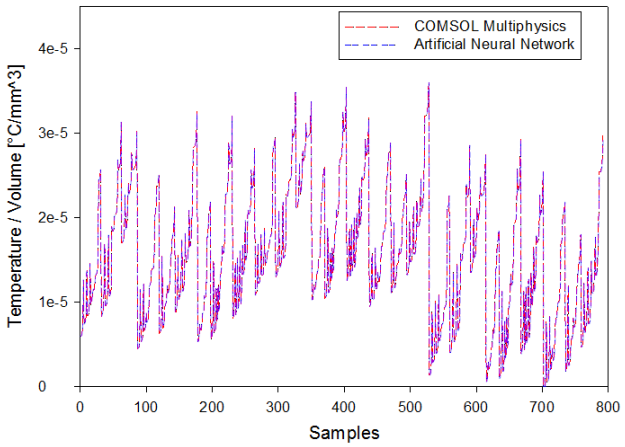

FIGURE 19. Maximum temperature variation according to the volume of the transformer body.

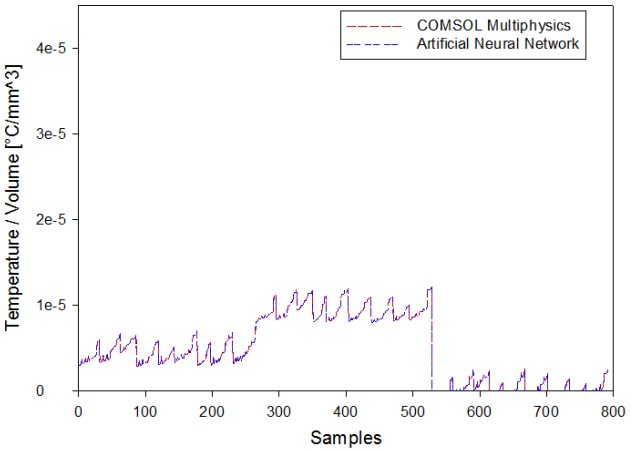

FIGURE 20. Minimum temperature variation according to the volume of the transformer body.

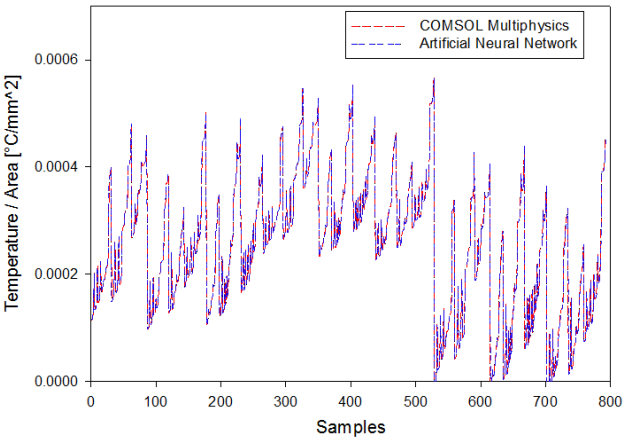

FIGURE 21. Maximum temperature variation according to the surface between the transformer body and environment.

was firstly measured. After one hour, the temperature at the low voltage winding was also measured.

Table 6 shows the input parameter values of the melt-resin medium voltage instrument transformer to which the heating test was applied.

TABLE 5. Sensitivity analysis results.

Variable	Description	MSE	S_i
X_{15}	Frequency (Hz)	593.0222	7667.8514
X_{12}	Turns per layer in the primary winding	267.1265	3453.9795
X_5	Primary winding inner diameter (mm)	247.362	3198.4216
X_{13}	Primary wire (AWG)	185.2046	2394.7188
X_{26}	Environment temperature (^{o}C)	161.326	2085.9652
X_{16}	Magnetic induction (Teslas)	111.1929	1437.7383
X_{23}	Losses in primary winding (W)	56.9998	737.0144
X_{24}	Losses in secondary winding (W)	54.8373	709.0537
X_{17}	Number of primary winding papers	50.7842	656.6454
X_{25}	Core losses (W)	15.9378	206.0777
X_2	Secondary voltage (V)	11.2674	145.6892
X_8	Secondary winding outer diameter (mm)	0.8926	11.5416
X_7	Secondary winding inner diameter (mm)	0.7799	10.0845
X_9	Primary winding height (mm)	0.6738	8.712
X_{22}	Applied test voltage (kV)	0.5441	7.0354
X_6	Primary winding outer diameter (mm)	0.4598	5.9447
X_{21}	Secondary resistance (Omega)	0.3785	4.8936
X_1	Primary voltage (V)	0.2328	3.0098
X_3	Number of primary turns	0.2293	2.9649
X_{20}	Primary resistance (Omega)	0.1975	2.5536
X_{18}	Primary wire cross-section (mm^2)	0.1147	1.4827
X_{19}	Secondary wire cross-section (mm^2)	0.0805	1.0412
X_4	Number of secondary turns	0.0773	1
X_{10}	Secondary winding height (mm)	0.0773	1
X_{11}	Primary winding layers	0.0773	1
X_{14}	Secondary wire (AWG)	0.0773	1

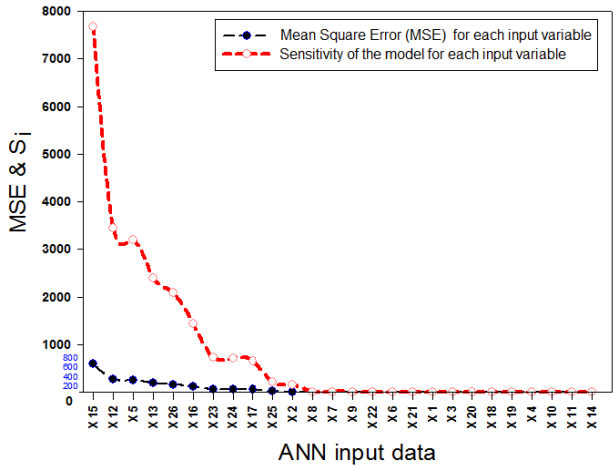

FIGURE 22. Sensitivity value and mse for each input variable.

Table 7 contains the results obtained during the laboratory heating tests, as well as the temperature results obtained from the ANN. It can be observed in Figure 25 that the maximum temperature in the transformer primary (Y_1) and secondary winding (Y_2) and the maximum contour temperature (Y_7), all of them obtained from the heating test, grows as magnetic induction and core losses increase. Figure 26 shows a similar behavior with data predicted by the ANN, with an increasing tendency in the temperature. The closeness of the values predicted by the ANN with the values obtained in the heating

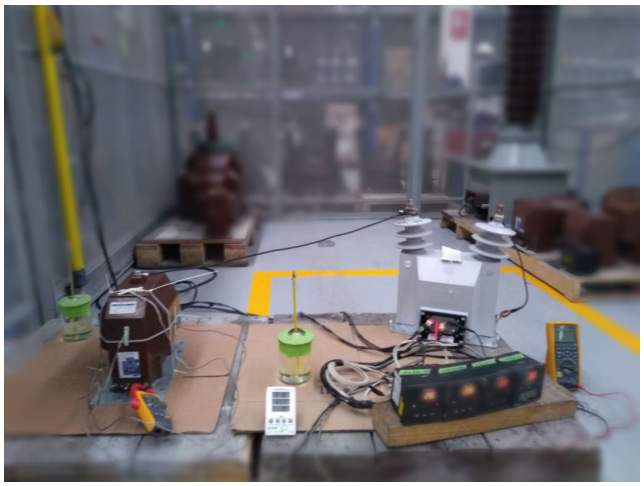

FIGURE 23. Instrument transformer during the heating test.

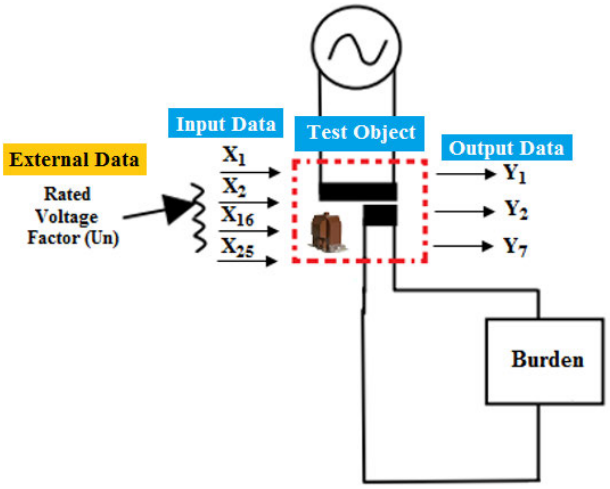

FIGURE 24. Test circuit for temperature measurement of instrument transformers.

test is showed in Figure 27, where both data sets follows the same pattern.

The values obtained from the heating test and the ANN show a MSE of 2.71% taking into account all measured values, therefore Y_1 has a corresponding MSE of 3.13%, Y_2 of 3.10% and Y_7 of 1.90%.

Where:

$$A = \left(\frac{X_1}{X_2}\right)(1.0),\quad B = \left(\frac{X_1}{X_2}\right)(1.2),\quad C = \left(\frac{X_1}{X_2}\right)(1.5),$$
$$D = \left(\frac{X_1}{X_2}\right)(1.7),\quad \text{and}\quad E = \left(\frac{X_1}{X_2}\right)(1.9).$$

VIII. CONCLUSION

This article introduces a new approach to predict the temperature of hot spots in the components of a cast resin dry-type instrument transformer. It provides a reference point for instrument transformer designers to identify the hot spots in the different components of the transformer. This approach starts with the transformer design by FEM; then, data obtained in the previous step are stored in a database; these values are used for training 1110 ANNs; finally,

TABLE 6. Input variables of the transformer under thermal test.

Input Variable	Name of the variable	Study parameter
X_1	Primary voltage (V)	7620
X_2	Secondary voltage (V)	120
X_3	Number of primary turns	15875
X_4	Number of secondary turns	250
X_5	Primary winding inner diameter (mm)	95.0
X_6	Primary winding outer diameter (mm)	132.44
X_7	Secondary winding inner diameter (mm)	65.0
X_8	Secondary winding outer diameter (mm)	75.782
X_9	Primary winding height (mm)	37.45
X_{10}	Secondary winding height (mm)	10.79
X_{11}	Primary winding layers	31.00
X_{12}	Turns per layer in the primary winding	528
X_{13}	Primary wire (AWG)	34
X_{14}	Secondary wire (AWG)	15
X_{15}	Frequency (Hz)	60
X_{16}	Magnetic induction (Teslas)	0.93, 1.11, 1.39, 1.57, 1.76
X_{17}	Number of primary winding papers	18
X_{18}	Primary wire cross-section (mm^2)	0.020
X_{19}	Secondary wire cross-section (mm^2)	1.651
X_{20}	Primary resistance (Ω)	4709.05
X_{21}	Secondary resistance (Ω)	0.577
X_{22}	Applied test voltage (kV)	38
X_{23}	Losses in primary winding (W)	13.877
X_{24}	Losses in secondary winding (W)	11.473
X_{25}	Core losses (W)	4.186, 5.014, 8.29, 11.36, 17.36
X_{26}	Environment temperature (^oC)	24

TABLE 7. Input variables of the transformer under thermal test.

Input Data			Output data (Temperature ^oC)					
			Y_1		Y_2		Y_7	
$\frac{X_1}{X_2}$	X_{16}	X_{25}	Test	ANN	Test	ANN	Test	ANN
A	0.93	4.18	67.78	66.32	70.61	69.02	50.71	49.72
B	1.11	5.01	68.74	67.13	71.56	70.02	51.47	50.26
C	1.39	8.29	72.33	70.3	76.18	73.96	53.8	52.43
D	1.57	11.36	74.91	73.22	79.16	77.6	56.47	54.83
E	1.76	17.36	81.4	79.41	87.13	85.33	61.85	60.28

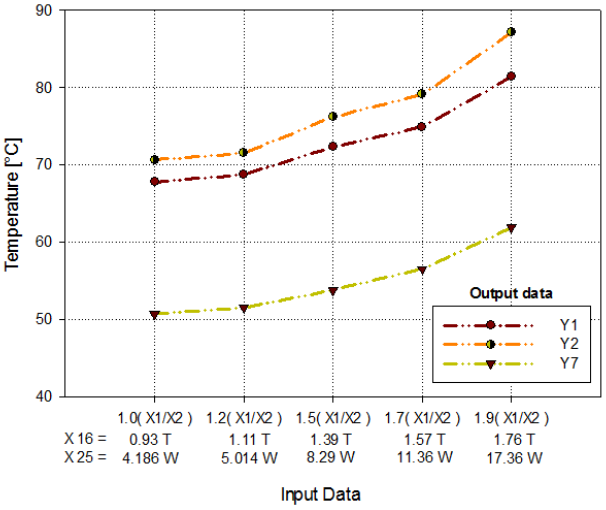

FIGURE 25. Maximum temperature obtained from the heating test with input variables indicated in Table 7.

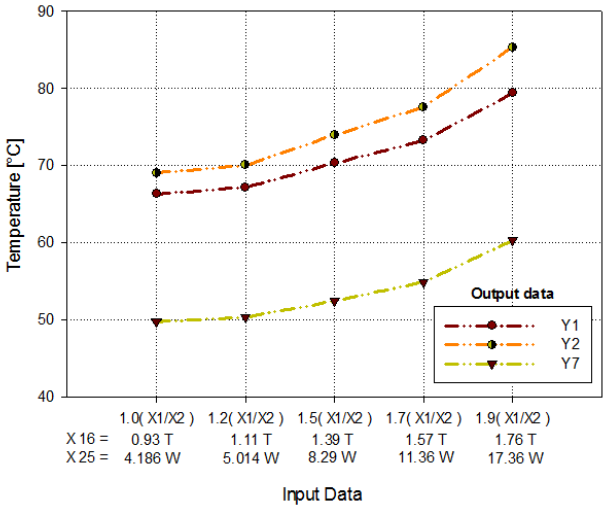

FIGURE 26. Maximum temperature obtained from the ANN with input variables indicated in Table 7.

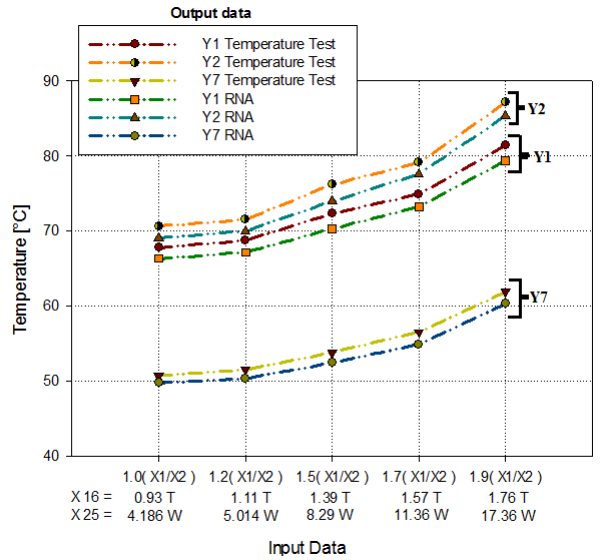

FIGURE 27. Maximum temperature obtained from the heating test and the proposed ANN with input variables from Table 7.

the ANNs with the best performance were validated with the data obtained from a physical model manufactured for this purpose. This methodology is the main contribution of this research article. The dependence of a lab and the transformer manufacturing is the unique limitation in this proposal, but with data obtained from simulations developed in COMSOL the ANNs can be validated. The best ANN shows accurate prediction with a MSE average of 2.71% with respect to the thermal tests. With the use of a large number of inputs in the design of the ANN in conjunction with the algorithm implemented to vary the number of hidden layers and the number of neurons for each hidden layer, we got an ANN with good performance (mean quadratic error = 0.003455) and a great correlation in the input/output data (R = 1). The variation of temperatures obtained from finite element simulations and those obtained from the ANN are very similar, and there is also a similarity pattern that depends on the volumetric and superficial dimensioning of each component of the transformer. Moreover, a transformer was manufactured in a laboratory of Arteche North America S.A. de C.V. in order to validate the results produced by the ANN, obtaining a MSE equal to 2.71%. With the results of this research work, the best ANN can be used together with optimization techniques to improve the efficiency and reliability of dry-type instrument transformers. As future work, this ANN will be used as the fitness function in an evolutionary algorithm to optimize the design of transformers.

APPENDIX

Nomenclature

3D	Three-dimension
ANN	Artificial Neural Networks
FEM	Finite Element Method
HL	Hidden layers
LMS	Least-Mean-Square
MSE	Mean Square Error
NN	Neurons per layer
ε	Emissivity of the surface (dimensionless quantity)
σ	Stefan Boltzmann's constant (W/(m^2 °C^4))
α	Absorptivity of the surface (dimensionless quantity)
C	Specific heat (J/(kg °C)
f	Frequency (Hz)
H	Convective heat transfer coefficient (W/(m^2 °C)
I_1	Current in the primary winding (A)
I_2	Current in the secondary winding (A)
k	Thermal conductivity (W/(m °C))
l_1	Length of the primary winding conductor (m)
l_2	Length of the secondary winding conductor (m)
MSE_i	Mean Square Error of predicted values without data for input variable X_i
P	Total losses of the transformer (W)
P_c	Total core losses (Watts/kg)
P_{cu}	Total winding losses due to the Joule effect (W)
P_{cu_1}	Primary winding losses (W)
P_{cu_2}	Secondary winding losses (W)
P_e	Eddy current losses in the core (W)
P_h	Hysteresis losses in the core (W)
Q	Heat source (W/m^3)
Q_{conv}	Heat transfer source per convection (W/m^2)
Q_{rad}	Heat transfer source per radiation (W/m^2)
R	Correlation between input and output data
R_1	Resistance of the primary winding conductor (Ω)
R_2	Resistance of the secondary winding conductor (Ω)
S_1	Conductor cross sectional area in the primary winding (m^2)
S_2	Conductor cross sectional area in the secondary winding (m^2)
S_i	Sensitivity of the model to variable X_i
T	Temperature (°C)
t	Time (s)

T_∞	Environment temperature (°C)
t_m	Network targets
T_s	Surface temperature (°C)
V	Volume of the heat source (m^3)
X_m	Network inputs for $m = 1,2,\ldots,26$
B	Flux density (T)
δ_e, δ_h	Constant depending on the type of core material
ρ	Mass density (kg/m^3)
ρ_1	Resistivity of the conductor in the primary winding (Ω.m)
ρ_2	Resistivity of the conductor in the secondary winding (Ω.m)
X_1	Primary voltage (V)
X_2	Secondary voltage (V)
X_3	Number of primary turns
X_4	Number of secondary turns
X_5	Primary winding inner diameter (mm)
X_6	Primary winding outer diameter (mm)
X_7	Secondary winding inner diameter (mm)
X_8	Secondary winding outer diameter (mm)
X_9	Primary winding height (mm)
X_{10}	Secondary winding height (mm)
X_{11}	Primary winding layers
X_{12}	Turns per layer in the primary winding
X_{13}	Primary wire (AWG)
X_{14}	Secondary wire (AWG)
X_{15}	Frequency (Hz)
X_{16}	Magnetic induction (T)
X_{17}	Number of primary winding papers
X_{18}	Primary wire cross-section (mm^2)
X_{19}	Secondary wire cross-section (mm^2)
X_{20}	Primary resistance (Ω)
X_{21}	Secondary resistance (Ω)
X_{22}	Applied test voltage (kV)
X_{23}	Primary winding losses (W)
X_{24}	Secondary winding losses (W)
X_{25}	Core losses (W)
X_{26}	Environment temperature (°C)
Y_1	Maximum temperature in primary winding (°C)
Y_2	Maximum temperature in secondary winding (°C)
Y_3	Maximum temperature in the insulation between primary and secondary winding (°C)
Y_4	Maximum core temperature (°C)
Y_5	Maximum temperature in the epoxy resin (°C)
Y_6	Minimum temperature in the epoxy resin (°C)
Y_7	Maximum contour temperature resin - environment (°C)

ACKNOWLEDGMENT

The authors would like to thank Ricardo Escutia, Marco Antonio Venegas, Verónica Vázquez, Arturo Aguilera, and Gustavo Alcantar for the support in the laboratory of Arteche North America S.A. de C.V.

REFERENCES

[1] S. Raetzke, M. Koch, and M. Anglhuber, "Modern insulation condition assessment for instrument transformers," in *Proc. IEEE Int. Conf. Condition Monitor. Diagnosis*, Sep. 2012, pp. 52–55, doi: 10.1109/CMD.2012.6416177.

[2] F. Nabhani, S. Hodgson, and K. Warnakulasuriya, "Estimation of temperature rise in MVA range dry-type transformers and practical verification based on simulated loading," in *Proceedings of the World Congress on Engineering*, vol. 1. London, U.K.: Newswood Limited, 2015, pp. 410–415. [Online]. Available: https://www.mendeley.com/catalogue/8e30670f-eea9-35b3-bc66-a154c788551b/?utm_source=desktop&utm_medium=1.19.4&utm_campaign=open_catalog&userDocumentId=%7Ba517de08-d00a-4e34-97a1-290bb40f2432%7D

[3] M. Eslamian, B. Vahidi, and A. Eslamian, "Thermal analysis of cast-resin dry-type transformers," *Energy Convers. Manage.*, vol. 52, no. 7, pp. 2479–2488, Jul. 2011, doi: 10.1016/j.enconman.2011.02.006.

[4] I. Soltanbayev, M. Bagheri, and T. Phung, "Real-time dry-type transformer aging evaluation," in *Proc. Int. Symp. Electr. Insulating Mater. (ISEIM)*, Sep. 2017, pp. 551–554, doi: 10.23919/ISEIM.2017.8166548.

[5] W. Ning and X. Ding, "Three-dimensional finite element analysis on fluid thermal field of dry-type transformer," in *Proc. 2nd Int. Conf. Instrum., Meas., Comput., Commun. Control*, Dec. 2012, pp. 516–519, doi: 10.1109/IMCCC.2012.128.

[6] M. F. de Gamboa, "Improved electrical voltage transformer," (in Spanish), Spain, Patent ES2 047 441, Oct. 16, 1996.

[7] G. Swift, T. S. Molinski, and W. Lehn, "A fundamental approach to transformer thermal modeling. I. theory and equivalent circuit," *IEEE Trans. Power Del.*, vol. 16, no. 2, pp. 171–175, Apr. 2001, doi: 10.1109/61.915478.

[8] A. C. Delaiba, J. C. de Oliveira, A. L. A. Vilaca, and J. R. Cardoso, "The effect of harmonics on power transformers loss of life," in *Proc. 38th Midwest Symp. Circuits Syst.*, Aug. 1995, pp. 933–936, doi: 10.1109/MWSCAS.1995.510243.

[9] S. Taheri, A. Gholami, I. Fofana, and H. Taheri, "Modeling and simulation of transformer loading capability and hot spot temperature under harmonic conditions," *Electr. Power Syst. Res.*, vol. 86, pp. 68–75, May 2012, doi: 10.1016/j.epsr.2011.12.005.

[10] S. Purushothaman and F. de Leon, "Heat-transfer model for toroidal transformers," *IEEE Trans. Power Del.*, vol. 27, no. 2, pp. 813–820, Apr. 2012, doi: 10.1109/TPWRD.2012.2185956.

[11] N. A. Muhamad, H. Kamarden, and N. A. Othman, "Heat distribution pattern of oil-filled transformer at different hottest spot temperature locations," in *Proc. IEEE 11th Int. Conf. Properties Appl. Dielectric Mater. (ICPADM)*, Jul. 2015, pp. 979–982, doi: 10.1109/ICPADM.2015.7295438.

[12] Q. Wen, Z. Baohui, H. Zhiguo, and B. Zhiqian, "Simulation and analysis of oil-immersed transformer based on thermal-fluid coupled field," in *Proc. Int. Conf. Power Syst. Technol.*, Oct. 2014, pp. 826–831, doi: 10.1109/POWERCON.2014.6993882.

[13] A. Y. Arabul and I. Senol, "Development of a hot-spot temperature calculation method for the loss of life estimation of an ONAN distribution transformer," *Electr. Eng.*, vol. 100, no. 3, pp. 1651–1659, Sep. 2018, doi: 10.1007/s00202-017-0641-0.

[14] D. Jia, Z. Yao, and C. Li, "The transformer winding temperature monitoring system based on fiber Bragg grating," *Int. J. Smart Sens. Intell. Syst.*, vol. 8, no. 1, pp. 538–560, 2015.

[15] C. Wei-Gen, L. Jun, W. You-Yuan, L. Liu-Ming, Z. Jian-Bao, and Y. Yan-Feng, "The measuring method for internal temperature of power transformer based on FBG sensors," in *Proc. Int. Conf. High Voltage Eng. Appl.*, Nov. 2008, pp. 672–676, doi: 10.1109/ICHVE.2008.4774024.

[16] W. Bengang, W. Xinye, Y. Zhoufei, and H. Hua, "A method of optimized neural network by L-M algorithm to transformer winding hot spot temperature forecasting," in *Proc. IEEE Electr. Insul. Conf. (EIC)*, Jun. 2017, pp. 87–91, doi: 10.1109/EIC.2017.8004603.

[17] M. Bagheri, A. Subramaniam, S. Bhandari, S. Chandar, S. Nadarajan, A. K. Gupta, and S. K. Panda, "Thermal prognosis of dry-type transformer: Simulation study on load and ambient temperature impacts," in *Proc. 41st Annu. Conf. IEEE Ind. Electron. Soc. IECON*, Nov. 2015, pp. 1158–1163, doi: 10.1109/IECON.2015.7392256.

[18] G. Yaman, R. Altay, and R. Yaman, "Validation of computational fluid dynamic analysis of natural convection conditions for a resin dry-type transformer with a cabin," *Thermal Sci.*, vol. 23, no. 1, pp. 23–32, 2019. [Online]. Available: https://hdl.handle.net/11363/1449

[19] Y. Cui, G. Wu, T. Saha, C. Ekanayake, and H. Ma, "Multi-physics modelling approach for investigation of moisture dynamics in power transformers," *IET Gener., Transmiss. Distrib.*, vol. 10, no. 8, pp. 1993–2001, May 2016, doi: 10.1049/iet-gtd.2015.1459.

[20] R. H. Perry, *Perry's Chemical Engineers Handbook*. New York, NY, USA: McGraw-Hill, 1997.
[21] L. R. Torin, D. O. G. Medina, and T. Sousa, "Dry-type power transformers thermal analysis with finite element method," *Int. J. Adv. Eng. Res. Sci.*, vol. 6, no. 3, pp. 159–165, 2019, doi: 10.22161/ijaers.6.3.19.
[22] S. Wang, Y. Wang, and X. Zhao, "Calculating model of insulation life loss of dry- type transformer based on the hot-spot temperature," in *Proc. IEEE 11th Int. Conf. Properties Appl. Dielectric Mater. (ICPADM)*, Jul. 2015, pp. 720–723, doi: 10.1109/ICPADM.2015.7295373.
[23] W. H. Tang, Q. H. Wu, and Z. J. Richardson, "A simplified transformer thermal model based on thermal-electric analogy," *IEEE Trans. Power Del.*, vol. 19, no. 3, pp. 1112–1119, Jun. 2004, doi: 10.1109/TPWRD.2003.822968.
[24] N.-C. Chereches, M. Chereches, L. Miron, and S. Hudisteanu, "Numerical study of cooling solutions inside a power transformer," *Energy Procedia*, vol. 112, pp. 314–321, Mar. 2017, doi: 10.1016/j.egypro.2017.03.1103.
[25] R. Guo, J. Lou, Z. Wang, H. Huang, B. Wei, and Y. Zhang, "Simulation and analysis of temperature field of the discrete cooling system transformer based on FLUENT," in *Proc. 1st Int. Conf. Electr. Mater. Power Equip. (ICEMPE)*, May 2017, pp. 287–291, doi: 10.1109/ICEMPE.2017.7982086.
[26] X. Zhang, Z. Wang, and Q. Liu, "Interpretation of hot spot factor for transformers in OD cooling modes," *IEEE Trans. Power Del.*, vol. 33, no. 3, pp. 1071–1080, Jun. 2018, doi: 10.1109/TPWRD.2017.2710087.
[27] T. Dao and B. T. Phung, "A study of hot-spot localization in distribution transformers," in *Proc. 1st Int. Conf. Electr. Mater. Power Equip. (ICEMPE)*, May 2017, pp. 36–40, doi: 10.1109/ICEMPE.2017.7982048.
[28] E. Cazacu, L. Petrescu, and V. Ionita, "Losses and temperature rise within power transformers subjected to distorted currents," in *Proc. 15th Int. Conf. Electr. Mach., Drives Power Syst. (ELMA)*, Jun. 2017, pp. 362–365, doi: 10.1109/ELMA.2017.7955464.
[29] R. A. Jabr, "Application of geometric programming to transformer design," *IEEE Trans. Magn.*, vol. 41, no. 11, pp. 4261–4269, Nov. 2005, doi: 10.1109/TMAG.2005.856921.
[30] E. Agheb and H. K. Høidalen, "Modification of empirical core loss calculation methods including flux distribution," *IET Electr. Power Appl.*, vol. 7, no. 5, pp. 381–390, May 2013, doi: 10.1049/iet-epa.2012.0368.
[31] AK Steel Corporation. (2019). *Grain Oriented Electrical Steels*. [Online]. Available: https://www.aksteel.com/sites/default/files/2019-10/litecarlite-and-mill-anneal.pdf
[32] E. A. Juárez, M. A. Venegas, J. C. Olivares-Galvan, I. A. Hernández, and J. L. Hernández-Avila, "Thermal analysis to locate the hotest point in a dry-type instrument transformer by using COMSOL multi-physics," (in Spanish), in *Proc. 8vo Congreso Internacional de Ingeniería Electromecánica y de Sistemas (CIIES)*, 2016, pp. 1–7.
[33] S. Tenbohlen, "Transformer reliability survey," *Brochure, Cigré*, vol. 642, pp. 1–57, Dec. 2011.
[34] W. Flores, E. Mombello, and G. Ratta, "Life of power transformers immersed in oil: State-of-the-art—Part II. Correlation between results of physical -Quimical tests," *IEEE Latin Amer. Trans.*, vol. 5, no. 8, pp. 591–598, Dec. 2007, doi: 10.1109/T-LA.2007.4445711.
[35] S. X. Wu and W. Banzhaf, "The use of computational intelligence in intrusion detection systems: A review," *Appl. Soft Comput.*, vol. 10, no. 1, pp. 1–35, Jan. 2010, doi: 10.1016/j.asoc.2009.06.019.
[36] M. Puig-Arnavat and J. C. Bruno, "Artificial neural networks for thermochemical conversion of biomass," in *Recent Advances in Thermochemical Conversion of Biomass*. Amsterdam, The Netherlands: Elsevie, 2015, pp. 133–156, doi: 10.1016/B978-0-444-63289-0.00005-3.

EDGAR ALFREDO JUAREZ-BALDERAS received the bachelor's degree and the Master of Science degree in electrical engineering with a specialty in control from the School of Mechanical and Electrical Engineering, National Polytechnic Institute, Mexico. He is currently pursuing the Ph.D. degree in advanced manufacturing with the Center for Advanced Technology (CIATEQ A. C.), Hidalgo, Mexico. He joined Arteche North America S. A. de C. V., in 2009, where he currently works as a Medium Voltage Development Engineer with the Research and Development Department.

JOSELITO MEDINA-MARIN received the M.S. and Ph.D. degrees in electrical engineering from the Research and Advanced Studies Centre, National Polytechnic Institute, Mexico, in 2002 and 2005, respectively. He is currently a Professor with the Advanced Research in Industrial Engineering Centre, Autonomous University of Hidalgo State, Pachuca, Hidalgo, Mexico. He is also a member of the National System of Researchers (SNI), where he is currently level 1. His current research interests include artificial neural networks, petri net theory and its applications, active databases, simulation, and programming languages.

JUAN C. OLIVARES-GALVAN (Senior Member, IEEE) received the Ph.D. degree in electrical engineering from CINVESTAV, Guadalajara, Jalisco, Mexico, in 2003. He was a Transformer Design Engineer with Electromanufacturas S. A. de C. V., Jalisco, for eight years. He was a Visiting Scholar with the Virginia Polytechnic Institute and State University, Blacksburg, VA, USA, in 2001 (one year); and a Visiting Professor with the University of Alberta, Edmonton, AB, Canada, in 2014 (one year). He is currently a Professor with the Departamento de Energia, Universidad Autónoma Metropolitana, (Azcapotzalco Campus), Mexico City, Mexico. His main research interests include experimental and numerical analyses of electromagnetic devices.

NORBERTO HERNANDEZ-ROMERO received the M.S. degree from the Department of Electrical Engineering, Laguna Technological Institute, Mexico, in 2001, and the Ph.D. degree from the Autonomous University of Hidalgo State, Pachuca, Hidalgo, Mexico, in 2009. He is currently a Professor with the Advanced Research in Industrial Engineering Centre, Autonomous University of Hidalgo State. He is also a member of the National System of Researchers (SNI), where he is currently level 1. His current research interests include system identification, feedback control design, genetic algorithms, fuzzy logic, neural networks, and its applications.

JUAN CARLOS SECK-TUOH-MORA received the M.S. and Ph.D. degrees in computer science from the Center for Research and Advanced Studies, National Polytechnic Institute, Mexico, in 1999 and 2002, respectively. He is currently a Professor-Researcher of the academic area of engineering with the Autonomous University of the State of Hidalgo. He is also a National Researcher Level 2 within the National System of Researchers of CONACYT. His current research interests include cellular automata, metaheuristics, evolutionary algorithms, and neural networks to model, design, optimize, and control engineering systems.

ALEJANDRO RODRIGUEZ-AGUILAR received the degree in industrial engineering and the Master of Science degree in manufacturing engineering from the Autonomous University of Hidalgo State, in 2007 and 2008, respectively. He is currently pursuing the Ph.D. degree in advanced manufacturing with the Center for Advanced Technology (CIATEQ A. C.), Hidalgo, Mexico. He currently works for Arteche North America S. A. de C. V., as a Low and Medium Voltage Development Engineer with the Research and Development Department.